frontiers | Frontiers in Oncology

TYPE Original Research
PUBLISHED 30 June 2023
DOI 10.3389/fonc.2023.1210487

OPEN ACCESS

EDITED BY
Leigh Ellis,
Cedars Sinai Medical Center, United States

REVIEWED BY
Daniel Gioeli,
University of Virginia, United States
Andrew Goldstein,
University of California, Los Angeles, United States

*CORRESPONDENCE
Justin M. Drake
jdrake@umn.edu

RECEIVED 22 April 2023
ACCEPTED 02 June 2023
PUBLISHED 30 June 2023

CITATION
White RE III, Bannister M, Day A, Bergom HE, Tan VM, Hwang J, Dang Nguyen H and Drake JM (2023) Saracatinib synergizes with enzalutamide to downregulate AR activity in CRPC. *Front. Oncol.* 13:1210487. doi: 10.3389/fonc.2023.1210487

Saracatinib synergizes with enzalutamide to downregulate AR activity in CRPC

Ralph E. White III[1], Maxwell Bannister[1], Abderrahman Day[2], Hannah E. Bergom[2], Victor M. Tan[3,4], Justin Hwang[2,5], Hai Dang Nguyen[1,6] and Justin M. Drake[1,5,6]*

[1]Department of Pharmacology, University of Minnesota, Minneapolis, MN, United States, [2]Department of Medicine, Division of Hematology, Oncology, and Transplantation, University of Minnesota, Minneapolis, MN, United States, [3]Institute for Quantitative Biomedicine, Rutgers, The State University of New Jersey, New Brunswick, NJ, United States, [4]Department of Pharmacology, Robert Wood Johnson Medical School, New Brunswick, NJ, United States, [5]Department of Urology, University of Minnesota, Minneapolis, MN, United States, [6]Member, Masonic Cancer Center, University of Minnesota, Minneapolis, MN, United States

Prostate cancer (PCa) remains the most diagnosed non-skin cancer amongst the American male population. Treatment for localized prostate cancer consists of androgen deprivation therapies (ADTs), which typically inhibit androgen production and the androgen receptor (AR). Though initially effective, a subset of patients will develop resistance to ADTs and the tumors will transition to castration-resistant prostate cancer (CRPC). Second generation hormonal therapies such as abiraterone acetate and enzalutamide are typically given to men with CRPC. However, these treatments are not curative and typically prolong survival only by a few months. Several resistance mechanisms contribute to this lack of efficacy such as the emergence of AR mutations, AR amplification, lineage plasticity, AR splice variants (AR-Vs) and increased kinase signaling. Having identified SRC kinase as a key tyrosine kinase enriched in CRPC patient tumors from our previous work, we evaluated whether inhibition of SRC kinase synergizes with enzalutamide or chemotherapy in several prostate cancer cell lines expressing variable AR isoforms. We observed robust synergy between the SRC kinase inhibitor, saracatinib, and enzalutamide, in the AR-FL+/AR-V+ CRPC cell lines, LNCaP95 and 22Rv1. We also observed that saracatinib significantly decreases AR Y^{534} phosphorylation, a key SRC kinase substrate residue, on AR-FL and AR-Vs, along with the AR regulome, supporting key mechanisms of synergy with enzalutamide. Lastly, we also found that the saracatinib-enzalutamide combination reduced DNA replication compared to the saracatinib-docetaxel combination, resulting in marked increased apoptosis. By elucidating this combination strategy, we provide pre-clinical data that suggests combining SRC kinase inhibitors with enzalutamide in select patients that express both AR-FL and AR-Vs.

KEYWORDS

prostate cancer, enzalutamide, SRC kinase inhibitor, Synergy, androgen receptor, phosphorylation

1 Introduction

Prostate cancer remains the highest diagnosed non-skin cancer amongst the American male population and is second highest in deaths, next to lung cancer. When primary prostate cancer is diagnosed in patients, many clinicians will either prescribe surgery, radiotherapy, and/or androgen deprivation therapy (ADT) that interfere with androgen synthesis such as leuprolide (GnRH agonist) (1). While potentially curative in up to 70-80% of men, the remaining 20-30% of men will develop tumors that become resistant to ADT with a rising prostate specific antigen termed castration resistant prostate cancer (CRPC). Newer, second generation therapies such as enzalutamide (AR competitive antagonist) (2, 3) and abiraterone acetate (CYP17A inhibitor) (4) have been developed to prolong survival in both hormone-naïve and hormone-resistant prostate cancer. However, none of these agents are curative, prompting investigators to elucidate the major mechanisms of resistance in CRPC.

Previous literature has implicated several major mechanisms of resistance in CRPC such as the amplification of the androgen receptor (AR), loss of *PTEN*, and *TMPRSS-ERG* fusions (5–7). One key mechanism is the emergence of androgen receptor splice variants (AR-Vs) (8). AR-Vs are constitutively-active truncated versions of AR that lack the C-terminal ligand binding domain and can function independently in the presence of androgen, leading to additional AR transcriptional activity. Clinically, AR-Vs (in particular AR-V7) increase in abundance and are implicated in resistance to prior hormonal therapies such as abiraterone acetate and enzalutamide (9). Recent studies show chemotherapy, such as docetaxel, has a higher treatment efficacy in patient tumors expressing AR-V7 (10). Yet, these therapies are toxic, leading to side effects that heavily impact quality of life for the patient. Chemotherapy also does not inhibit primary mechanisms of resistance involving AR, revealing the need for alternative approaches to treatment.

Another mechanism of resistance is increased tyrosine kinase signaling (11). Our previous work evaluated the phosphoproteome of CRPC patients at autopsy. Using multi-omic integration, we took a kinase-centric approach to identify SRC kinase as a key activated kinase and signaling hub in CRPC (12). SRC kinase, also known as c-SRC, is a non-receptor tyrosine kinase that plays major roles in cancer cell proliferation, communication, and adhesion (13, 14). Specifically to prostate cancer, SRC kinase phosphorylates AR at Y^{534} (15) and directly interacts with the AR N-Terminal domain *via* hydrophobic interactions with SRC's SH3 domain (16). Phosphorylation of AR by SRC kinase maintains AR stability and transcriptional activity (17, 18) along with regulating other kinases that phosphorylate other residues of AR *via* growth factor stimulation and kinase crosstalk (19–21). While intriguing as a pre-clinical target, SRC kinase inhibition in clinical trials for treatment of CRPC has not been successful (22). Administration of a dual SRC kinase and BCR-ABL inhibitor, dasatinib, failed in late stage CRPC clinical trials as both a monotherapy and in combination with docetaxel (23). These clinical trial results dampened the excitement around SRC kinase as a viable target in CRPC. However, several explanations may exist as to why these trials were not successful, such as lack of patient stratification and broadly targeted combinations that do not focus on AR inhibition.

To resolve this, in this study, we provide pre-clinical data that supports SRC kinase inhibition with standard of care hormonal therapies such as enzalutamide for treating AR positive (AR+) CRPC. We find that enzalutamide plus saracatinib was strongly synergistic in AR-full length positive (AR-FL+) cell lines, regardless of AR-V positive (AR-V+) status. Meanwhile, docetaxel plus saracatinib was not as effective, especially in cell lines expressing AR-Vs, supporting the potential failure of dasatinib in the previously mentioned clinical trial with docetaxel. We also found that saracatinib ablated AR Y^{534} phosphorylation, AR-V protein expression, and altered AR specific gene signatures, suggesting that AR stability and transcriptional activity were perturbed through SRC kinase inhibition. Lastly, we also observed that saracatinib induced higher levels of γH2AX, DNA replication stress when in combination with enzalutamide, and markers of apoptosis in the AR-FL+/AR-V+ cell line 22Rv1.

2 Results

2.1 Enzalutamide and saracatinib yields strong synergy in AR-FL+/AR-V+ cell lines

To begin studying our drug combinations, we selected prostate cancer cell lines with different AR genetic backgrounds that also express SRC kinase (Figure 1A), expecting a myriad of responses that will allow us to evaluate synergy between our selected drugs. Using these cell lines, we generated dose-response curves to determine the IC50s of enzalutamide (enza), docetaxel (DTX), and the SRC kinase inhibitor saracatinib (sara) (Figure 1B). Using the IC50 dosage, we administered serial dilutions of enza plus sara or DTX plus sara to our cell lines (Supplemental Figure 1A). Synergy was then calculated *via* Bliss Independence (BI) and the Combination Index (CI) equation *via* Chou-Talalay method through CompuSyn 1.1 (24, 25). AR-FL+ only AD1 cells showed synergy in both enza plus sara and DTX plus sara combinations (Figure 1C; Supplemental Figure 1B). Synergy was also observed in both AR-FL+ and AR-V+ 22Rv1 and LNCaP95 cells (Figures 1D, E; Supplemental Figure 1B) with the enza plus sara combination. Interestingly, synergy was observed in LNCaP95 cells with the DTX plus sara combination but not in 22Rv1 cells. AR-V+ R1D567 cells showed synergy in the enza plus sara combination *via* the BI model (Figure 1F) and showed additivity *via* the CI model (Supplemental Figure 1B). There is a lack of synergy seen between DTX plus sara in R1D567 using both models (Figure 1F; Supplemental Figure 1B). Using CompuSyn 1.1, we were able to generate a dose reduction index (DRI), which determines the fold reduction of each drug when in combination with another drug. In our 22Rv1 and LNCaP95 cell lines, we see a reduction up to 5-fold for both enza and sara when in combination (Supplemental Figure 1C). We also observe a 3-fold reduction for DTX and a near zero fold reduction for sara when in combination, which suggests that the reduction of sara was more potent in the presence of enza versus DTX. Lastly, we

10.3389/fonc.2023.1210487

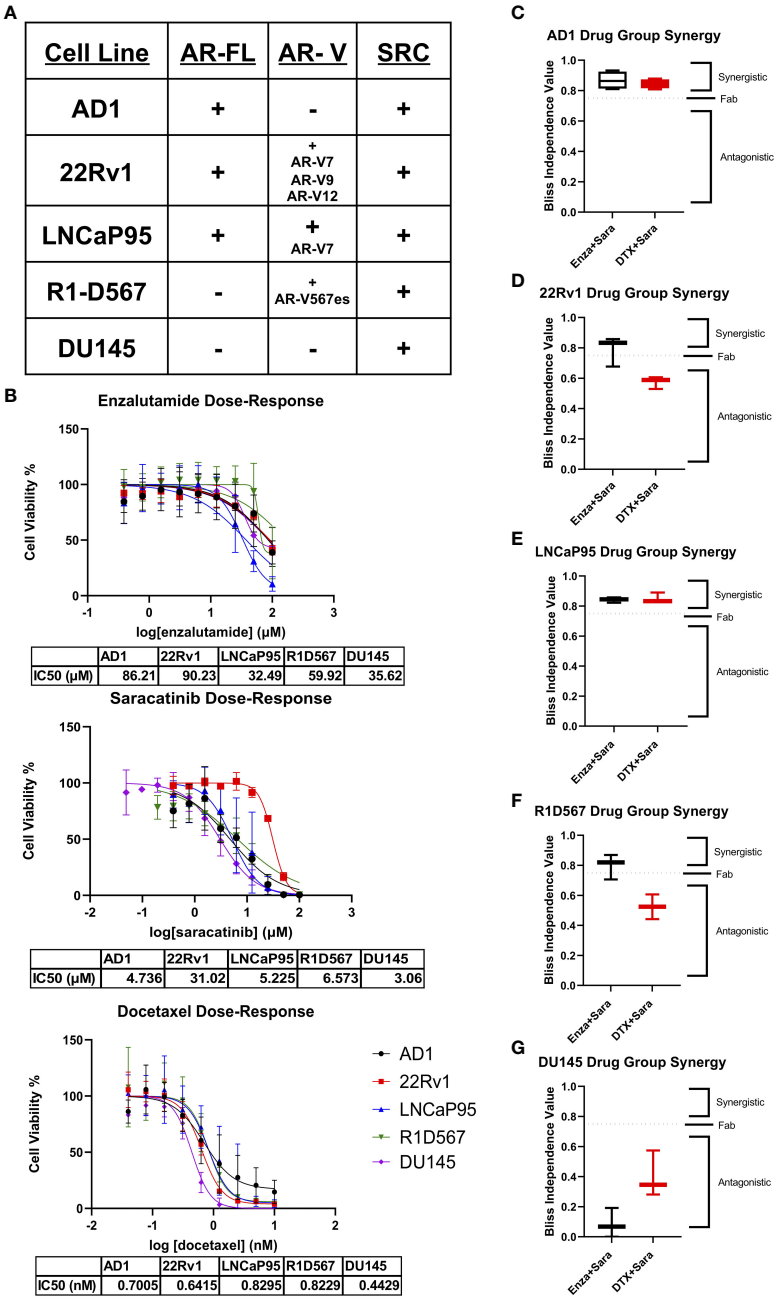

FIGURE 1
Synergy observed between Enzalutamide and SRC kinase Inhibitors in AR+ Positive Cell Lines. **(A)** Cell lines used for *in vitro* studies and their corresponding AR status and SRC status. **(B)** Dose-response curves for Enzalutamide (Enza), Saracatinib (Sara), and Docetaxel (DTX) for each cell line. IC50 dosage of each drug to each cell line used is shown below each curve (N≥ 3). **(C–G)** Bliss independence results for drug combos for cell lines AD1, 22Rv1, LNCaP95, R1D567, DU145. Dosage for each drug for each cell line is as follows: AD1- Enza: 86 μM Sara: 5 μM DTX: 0.70 nM, 22Rv1- Enza: 90 μM Sara: 31 μM DTX: 0.64 nM LNCaP95- Enza: 32.5 μM Sara: 5.2 μM DTX: 0.83 nM, R1D567- Enza: 60 μM Sara: 6.6 μM DTX: 0.82 nM, DU145- Enza: 36 μM Sara: 3 μM DTX: 0.44 nM. N≥3 for all cell lines except LNCaP95 where N=2.

show no synergy, but rather antagonism, between enza plus sara and DTX plus sara in the AR negative DU145 cells (Figure 1G). We expected no synergy for enza plus sara in DU145 cells due to enza's inability to enact its mechanism of action because of DU145's lack of AR. Overall, these findings indicate there is substantial synergy between enza and sara in PCa cell lines and this synergy potentially coincides with the presence of AR-FL alone or in the presence of AR-V expression.

2.2 Saracatinib decreases AR phosphorylation and AR-V protein expression *via* SRC kinase inhibition

Previous literature has shown that certain kinases can regulate AR function, stability, and activity *via* phosphorylation on particular residues of AR. For example, CDK1/5/9 phosphorylates AR S^{81}, which is located within the N-terminal domain of AR and

10.3389/fonc.2023.1210487

regulates AR transactivation, transcription, and nuclear localization (26–28). SRC kinase phosphorylates AR on residue Y^{534}, which is critical for AR stability and transcription (17, 18). To assess the role of SRC kinase inhibition on AR phosphorylation and how that may contribute to drug synergy in CRPC, we seeded the CRPC cell lines 22Rv1 and LNCaP95 overnight followed by a media change to charcoal stripped serum media for 3 days. We then administered individual drug and drug combinations for 24 hours at each drug's IC50 followed by stimulation with R1881, a synthetic androgen, and epidermal growth factor (EGF) for 5 minutes to induce maximal phosphorylation on AR. We found that sara ablated the phosphorylation of AR Y^{534} (both AR-FL and AR-Vs) in both 22Rv1 and LNCaP-95 cells (Figures 2A, B). This effect was sara dependent as enzalutamide and docetaxel were unable to decrease this phosphorylation site, while sara alone and in combination with enza or DTX all produced similar reduction of this phosphorylation residue. We also measured AR S^{81} phosphorylation and found that its reduction coincided with the reduction of AR protein. Interestingly, we also found that total AR-V protein expression was decreased by sara, so we measured AR-V7 and found decreased

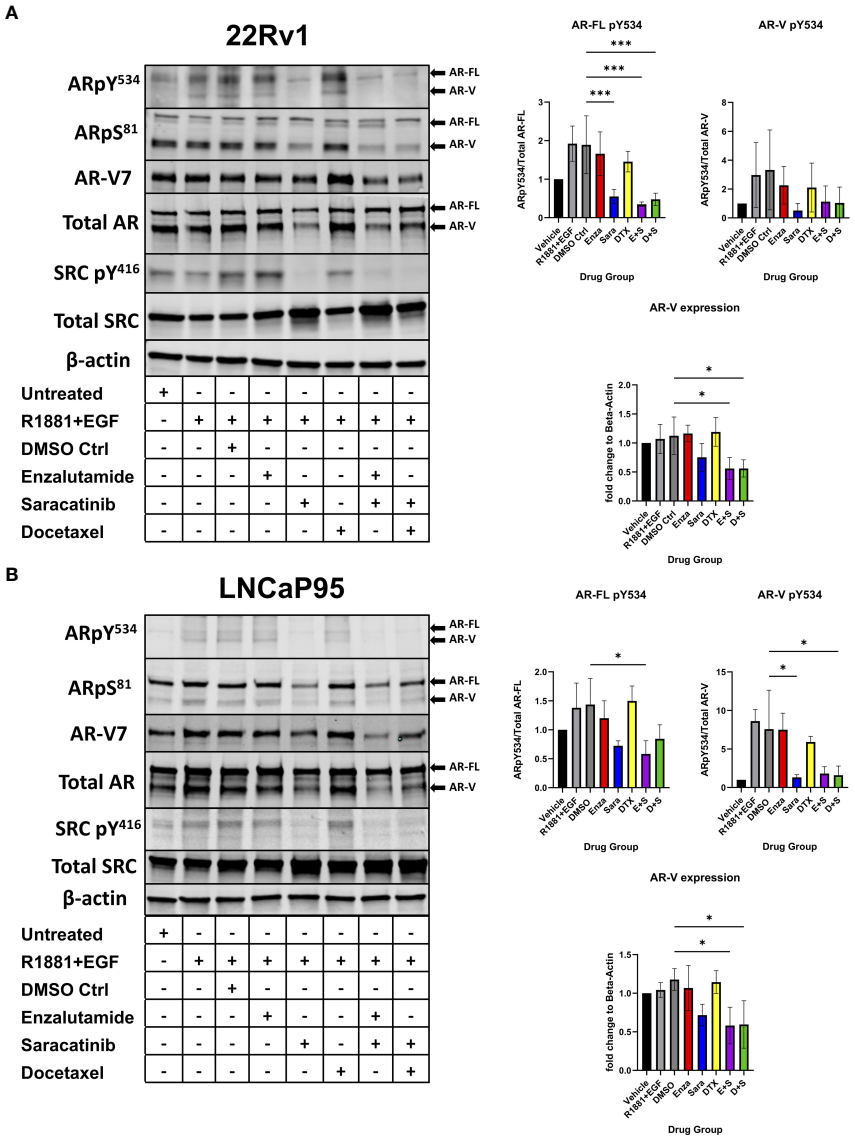

FIGURE 2
AR Y^{534} phosphorylation and AR-V protein expression ablated *via* SRC kinase inhibition. **(A)** 22Rv1 and **(B)** LNCaP95 cells are seeded in FBS media for 24 hrs then switched to Charcoal-Stripped Serum (5%) RPMI Media and grown over 3 days. Cells are then given the drugs for 24hrs and stimulated with R1881, a synthetic androgen, and Epidermal growth factor (EGF) for 5 minutes. Drug groups are DMSO, Enza, Sara, DTX, Enza plus Sara (E+S), and DTX plus Sara (D+S). Dosage for each drug for both cell lines is as follows: 22Rv1- Enza: 90 μM Sara: 31 μM DTX: 0.64 nM LNCaP95- Enza: 32.5 μM Sara: 5.2 μM DTX: 0.83 nM. Blotting for AR, SRC, ARpY534, ARpS81, SRCpY416, β-actin (N≥ 3) and ARv7 (N=2). *, $P < 0.05$; and ***, $P < 0.001$.

10.3389/fonc.2023.1210487

expression in sara-treated samples. Overall, these findings indicate that pharmacological ablation of SRC kinase can heavily affect AR phosphorylation and AR protein expression.

2.3 Saracatinib alters AR gene signature in CRPC

Based on previous literature that stated phosphorylation on AR Y^{534} regulated AR transcriptional activity, we decided to perform RNA-seq to evaluate the consequence of AR-specific gene signatures after sara-induced reduction of AR Y^{534} phosphorylation. 22Rv1 cells were prepared as stated previously and administered drug groups (enza, sara, enza plus sara). Cells were harvested after 48 hours and RNA sequencing was performed. We initially focused on changes in steroid receptor mRNA expression as it had been reported that the inhibition of AR can induce expression of another steroid receptor as a mechanism of resistance to AR targeted therapies, such as with the glucocorticoid receptor (NR3C1) and mineralocorticoid receptor (NR3C2) (29, 30) We also utilized gene signatures from select literature. We found that sara reduced AR mRNA expression (Figure 3A) and enza induced the expression of the glucocorticoid-GR (NR3C1) and mineralocorticoid-MR (NR3C2) receptors, similar to what was published previously. We also found that the enza plus sara combination further reduced AR mRNA expression with little induction of NR3C1 and NR3C2 expression, hinting towards sara preventing this mechanism of resistance. To investigate this further, we used the Sawyers GR gene signature (29) and observed that enza and sara individually, as well as in combination, reduced the

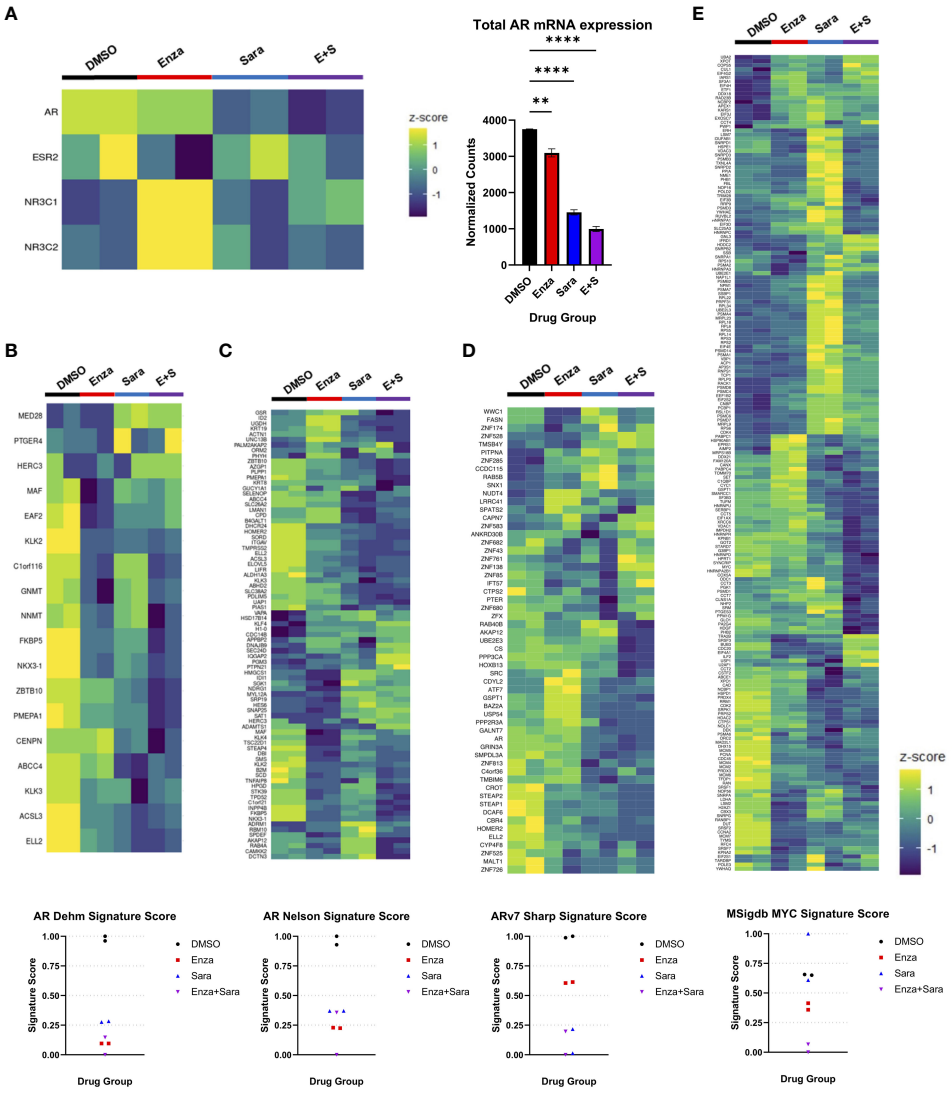

FIGURE 3
Saracatinib affects AR gene signatures. 22Rv1 cells seeded in FBS media for 24 hrs then switched to Charcoal-Stripped Serum (5%) RPMI Media and grown over 3 days. Cells are then given the drugs, R1881, and EGF for 48hrs. Drug groups are DMSO, Enza, Sara, or E+S. **(A)** Heatmap showing steroid receptor gene expression (left) with corresponding bar graph showing normalized counts of AR mRNA expression (right). **(B)** Heatmap of Dehm AR gene signature (19 genes) corresponding to AR activity with signature score **(C)** Heatmap of Nelson AR gene signature (83 genes) with signature score **(D)** Heatmap of Sharp AR-V7 gene signature (59 genes) **(E)** Heatmap of MSigdb MYC gene signature (200 genes). Dosage for each drug for this cell lines is as follows: 22Rv1- Enza: 90 μM Sara: 31 μM DTX: 0.64 nM N=2 **, $P < 0.01$; and ****, $P < 0.0001$.

signature score (Supplemental Figure 2B). This suggests that enza and sara work together to prevent the transcription of genes involved in GR dependent mechanisms of resistance (e.g BCL6, ZMIZ1, SGK1, MEAF6). We also observed that sara altered AR gene signature activity in both the Dehm (31) and Nelson (32) AR-regulated gene sets. In the Dehm gene set, which contains 19 AR-regulated genes, we found that sara treatment alone reduced certain AR-regulated genes (e.g. ABCC4, KLK3, ACSL3, and ELL2) and the combination of sara and enza dramatically reduced the expression of several AR-regulated genes that were less perturbed by either treatment alone, including ZBTB10, PMEPA1, CENPN, NKX3-1, and FKBP5 (Figure 3B). Similar effects were also observed in the Nelson gene set with sara affecting unique AR-regulated genes when compared to the sara plus enza combination. We also found that sara can reduce the AR-regulated gene signature scores in both the Dehm and Nelson gene sets similar to enza and that the combination of enza plus sara even further reduced the AR activity signatures scores in both datasets (Figures 3B, C). We then evaluated the protein expression of AR targets FKBP5 and NKX 3.1 and found that enza and sara individually, and in combination, reduced their protein expression in line with our RNA sequencing data (Supplemental Figure 2A). We also assessed AR-V7-specific, cell proliferation, and cell cycle gene signatures. We found that sara drastically altered the Sharp AR-V7 gene signature (33) more than enza, affecting pivotal regulatory genes of AR-V7, such as HOXB13 and FASN, with a reduction in the AR-V7 signature score (Figure 3D). For the MYC gene signature, we observed sara-specific changes in MYC-related genes opposite from DMSO control (Figure 3E). Interestingly, this did not dramatically affect the MYC signature score but when added in combination with enza, we observed a significant drop in the MYC signature score suggesting the potency of this combination. Lastly, we observed that sara and enza dramatically altered the G2M gene signature leading to a significant drop in its signature score (Supplemental Figure 2C). Overall, these findings indicate that SRC kinase ablation can heavily affect AR-dependent gene expression and may work with enzalutamide to further inhibit AR-specific activity.

2.4 Saracatinib induces DNA damage and apoptosis *via* DNA replication stress

Since sara alone and in combination with enza significantly lowered AR activity signature scores, and that blocking AR function can induce cell death *via* apoptosis and suppression of cell growth (34–36), we sought to investigate if sara plus enza synergized in exerting their cytotoxic effects during the cell cycle and activating apoptotic pathways. First, to follow the cell cycle status of individual cells in asynchronous growing cell populations, we stained for the chromatin-bound PCNA, a component of the DNA replication fork, and DNA in the 22Rv1 cell line using antibody and DAPI, respectively (Supplemental Figure 2A, left; Figure 4A). We also pulse-labeled newly synthesized DNA with EdU, a modified thymidine nucleoside incorporated into the DNA of actively proliferating cells. Cells undergoing DNA replication displayed high levels of chromatin-bound PCNA and became EdU-positive after pulse-labeling. We then established a cell cycle profile using quantitative image-based cytometry, comparing PCNA and DAPI in each drug group to identify G1, S, and G2 cell populations (Supplemental Figure 2A, left). Sara treatment alone and in combination with enza or DTX, caused a modest, but statistically significant, decrease in S phase cells (Supplemental Figure 2A, right). We then evaluated our drug combinations' impact on DNA synthesis by measuring pulse-labeled EdU in PCNA-positive cells. In S phase cells (PCNA-positive), enza and sara individually decreased EdU incorporation in comparison to DTX (Figure 4B). We also saw enza plus sara decreases EdU incorporation to baseline in comparison to DTX plus sara, showing enza plus sara can greatly halt DNA synthesis. With DNA synthesis impacted, this may lead to DNA damage in S phase. We measured H2AX phosphorylation on residue S^{139}, also known as γH2AX, a known marker for DNA damage. We found that the sara alone and in combination with enza or DTX significantly induced higher levels of γH2AX in S phase cells (Figure 4C). Also, γH2AX expression was not specific to any one cell cycle population, as sara alone and in combination with enza or DTX caused greater amounts of γH2AX in G1 cells (Supplemental Figure 2B, left), while enza plus sara induced the highest amounts of γH2AX in G2 cells (Supplemental Figure 2B, right). Lastly, to understand activation of apoptotic pathways, we measured activated caspase 3/7 and cleaved PARP, early markers for apoptosis required for late stages in apoptosis. We detected higher levels of activated caspase 3/7 in the enza plus sara combination over each drug alone (Figure 4D) as well as higher cleaved PARP expression (Figure 4E). Overall, these findings indicate SRC kinase inhibition *via* sara causes DNA replication stress that is supplemented more by enzalutamide vs. docetaxel, resulting in greater activation of apoptotic pathways.

3 Discussion

In this study, we found that enzalutamide plus saracatinib is synergistic in prostate cancer cell lines that express AR-FL, regardless of AR-V status. We also found that docetaxel plus saracatinib is synergistic to additive in cell lines that express AR-FL only. However, synergy is reduced between docetaxel and saracatinib in cell lines that express AR-Vs, highlighting its treatment potential in the correct context. Clinically, this is important for the patient as we can identify the appropriate combination strategy to have a greater impact on halting their disease progression and circumvent any unnecessary side effects. However, this study remains correlative and lacks genetic validity, requiring further investigation to understand how AR status can affect therapeutic efficacy with our combination of drugs in PCa cells. Under castrate conditions, AR can shift from its canonical ligand dependent signaling to non-canonical ligand independent signaling (15, 37, 38). This adaptive signaling can lead to the expression of constitutively active AR-Vs and increased tyrosine kinase activity. SRC kinase phosphorylates AR and has been shown to bind to the N-Terminal domain of AR, leading to a gain in cell proliferation and signaling (15). We found that saracatinib decreased AR Y^{534}

10.3389/fonc.2023.1210487

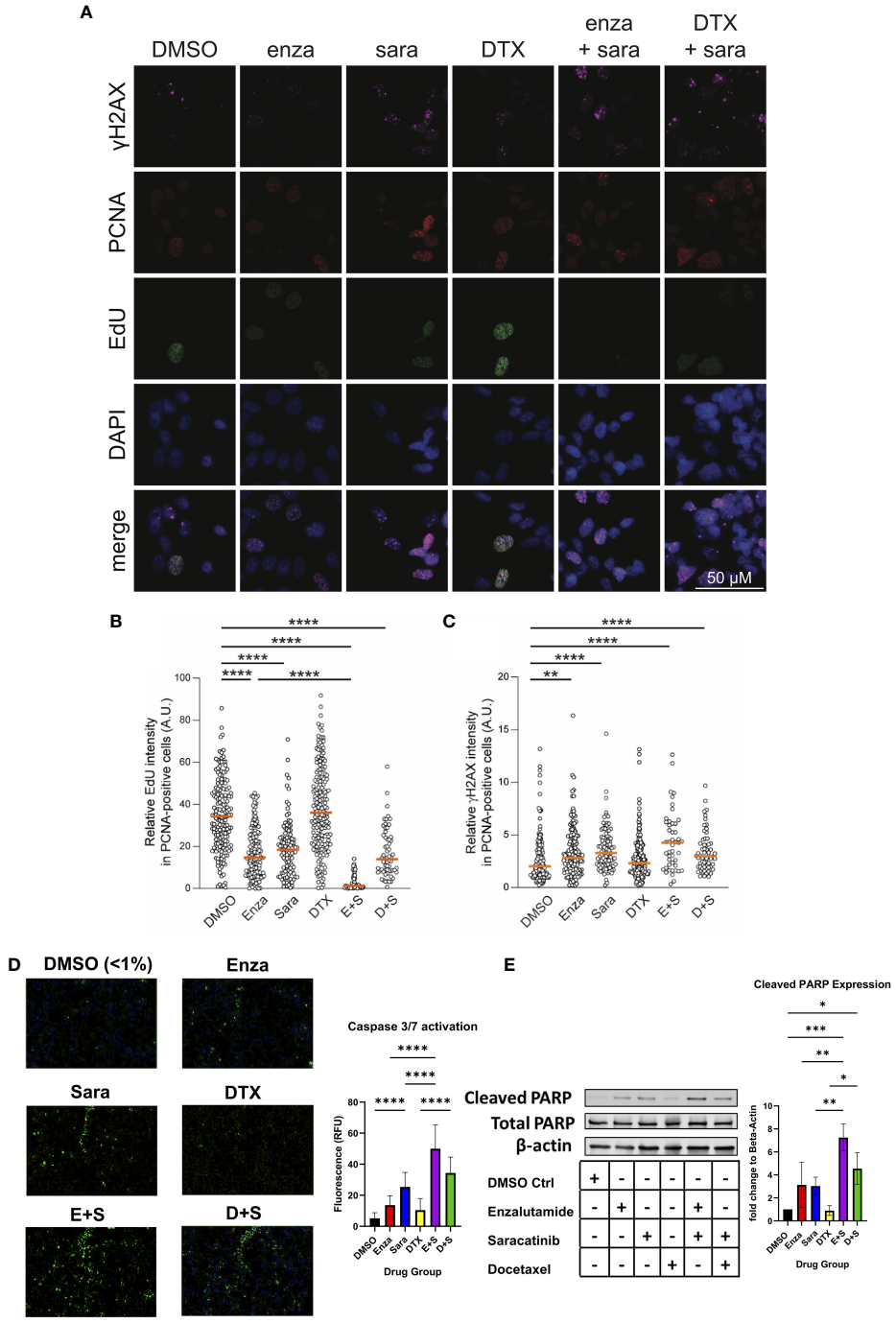

FIGURE 4
Saracatinib halts DNA synthesis, induces DNA Damage and activates markers of apoptosis. **(A)** Representative images of charcoal-stripped 22Rv1 cells treated with DMSO, Enza, Sara, DTX, E+S, or D+S, for 24 hrs then stained for indicated antibodies. **(B)** EdU (via Click-It) and **(C)** γH2AX quantification. **(D)** Caspase 3/7 activation (via Cell Event) representative images, detected *via* immunofluorescence with quantification. **(E)** Western blot of Cleaved PARP, Total PARP, and β-actin. Dosage for each drug for this cell lines is as follows: 22Rv1- Enza: 90 μM Sara: 31 μM DTX: 0.64 nM N=3. *, $P < 0.05$; **, $P < 0.01$; ***, $P < 0.001$; and ****, $P < 0.0001$.

phosphorylation on both AR-FL and AR-Vs and, interestingly, saracatinib also decreased AR-V protein expression, including AR-V7. This points out that changes in phosphorylation on AR Y^{534} may affect AR-V protein stability highlighting a possible route towards its ligand-independent function.

Previous literature has shown that the phosphorylation of AR can activate and contribute to AR-dependent gene networks (26–28, 38). In particular, Y^{534} phosphorylation by SRC kinase contributes to AR transcriptional activity and nuclear localization (21). Therefore, we evaluated saracatinib's effects on AR mRNA expression alongside other

steroid receptors' mRNA expression. We found that AR mRNA expression decreased in the presence of saracatinib while GR and MR mRNA expression increased when enzalutamide was given. The effect of enzalutamide is blunted when combined with saracatinib, suggesting that saracatinib affects AR-gene regulated specific mechanisms of resistance tied to enzalutamide. We also found that enzalutamide and saracatinib individually, and in combination, negatively altered the GR gene signature. We then evaluated AR gene signatures to observe saracatinib's effects on AR-dependent genes and observed that saracatinib altered AR gene signature scores to a similar level as enzalutamide, which was quite surprising. We found many of the major AR target genes were impacted, such as TMPRSS2, KLK2/3, NKX3.1 and FKBP5. In addition, we evaluated AR-V7 specific, MYC, and G2M gene signatures and found saracatinib negatively altered AR-V7 and G2M gene signatures, while having an opposite effect to DMSO in the MYC signature. While this mechanism requires more investigation, we postulate that saracatinib impacts AR-V protein stability, resulting in reduced AR-V binding to DNA that in return lessens activation of ligand-independent AR gene expression.

AR inhibition has been shown to cause DNA damage on telomeres to prostate cancer cells in previous literature (34, 36), so we evaluated our drug combinations in DNA synthesis, DNA damage, and apoptosis. Using quantitative immunofluorescence cytometry, we identified G1, S phase, and G2 cell populations in each of our drug groups and found that saracatinib decreased the percentage of cells in S-phase. We also observed that enzalutamide and saracatinib, individually and together, halted EdU incorporation greater than docetaxel alone, indicating that cells undergo DNA replication stress when given this drug combination. We also found that saracatinib induced greater γH2AX expression vs. enzalutamide or docetaxel. Lastly, we found greater caspase 3/7 activity and cleaved PARP expression in cells administered enzalutamide and saracatinib.

While the *in vitro* mechanisms combining saracatinib plus enzalutamide are quite striking and point towards SRC kinase as a key therapeutic target in CRPC, clinical trial data has been not as positive. In the phase 3 clinical trial, READY, docetaxel plus the dual SRC kinase and BCR-ABL inhibitor, dasatinib, were given to metastatic CRPC patients who were naïve to chemotherapy (23). While the trial was unable to meet the specified primary endpoints and no benefit in overall survival, it should be noted that there was a lack of CRPC patient stratification by AR or SRC kinase status. It should also be pointed out that while docetaxel is a standard of care in CRPC (9), it does not directly affect AR function or activity. From a clinical perspective and our work presented here, the combination of enzalutamide plus saracatinib would benefit a portion of CRPC patients who still retain AR activity, including AR-Vs, over docetaxel plus saracatinib. Our study may also prompt investigators to look deeper into select kinases that phosphorylate AR, such as CDK1/5/9, ACK1, SRC, MAPK (21), as inhibition of these kinases in AR+ prostate cancers may provide patient benefit in combination with AR-targeted agents.

Evaluating combination therapy by using mathematical equations such as Bliss Independence and Combination Index, can possibly bridge the clinical gap for testing (39). Both equations note trends of synergy and the interplay of the drugs' mechanisms of actions based on the cell model (24, 25). Specifically, for our purposes, we focused on AR species as the variable of our models and saw different responses with enzalutamide and docetaxel when paired with saracatinib. While enzalutamide combinations were synergistic and resulted in greater prostate cancer cell death, it is still important to note that docetaxel combinations were synergistic to additive in some of our models, citing the importance of using docetaxel in the clinic in some cases, especially when AR-Vs are not expressed.

Major topics of interest to build upon these findings involve the accessibility of AR and deciphering the mechanism of DNA damage caused by saracatinib. Since saracatinib alters AR transcriptional activity, SRC kinase inhibition could cause chromatin remodeling of AR as well as affect co-activator recruitment, as shown in previous literature with CDKs (27). Saracatinib's induction of γH2AX is of key importance to determine if saracatinib causes DNA replication forks and how that impacts DNA repair pathways. Overall, we present SRC kinase inhibition as a therapeutic strategy to be combined with current AR therapies available for use to treat AR driven CRPC. Though we show this promising pharmacological intervention, there are limitations. With SRC kinase inhibitors, like many kinase inhibitors, they are promiscuous which lead to off target effects. This prompts a need to develop better kinase inhibitors with specificity to the chosen kinase target. Also, while saracatinib is a potent SRC kinase inhibitor, it also inhibits other members of the SRC family kinases, including Lyn and Fgr, which are also expressed in prostatic tissue. This requires further investigation into each kinases' activity and how their inhibition could impact prostate cancer cell death.

4 Methods

4.1 Cell culture

Human prostate cancer cell lines DU-145, 22Rv1, LNCaP95 were obtained from ATCC and cultured according to ATCC protocol in RPMI1640, supplemented with 10% FBS and 1% penicillin-streptomycin and 1% Glutamax, a substitute for L-glutamine (Corning). AD1 and R1D567 cells were obtained from Dr. Scott Dehm at the University of Minnesota Medical School and cultured as described previously (40). Cells were not used beyond 25 passages. All cells were grown and maintained in a humidified incubator at 37°C and 5% CO2.

4.2 Drug dose response (cell viability)

Cells were seeded at the following densities: DU-145 (500 cells/0.1 mL), AD1 (2,000 cells/0.1 mL), R1D567 (1,000 cells/0.1 mL), LNCaP95 (4,000 cells/0.1 mL), 22Rv1 (2,000 cells/0.1 mL) in 96 well plates in RPMI media (Sigma-Aldrich) with 10% FBS, 1% penicillin-streptomycin, and 1% Glutamax (Corning). After an overnight incubation at 37°C and 5% CO2, media in the wells was replaced with fresh RPMI media with 5% charcoal-stripped (CSS)-FBS, 1% penicillin-streptomycin, and 1% Glutamax

(Corning). Cells were then grown in the media for 3 days. One of the following three drug groups is then administered: enzalutamide, saracatinib, ranging from 0.39-100μM, and docetaxel 0.04-10nM. All drugs were obtained from Selleckchem. Treatment lasted for 6 days with replenishment of the media and drug after 3 days. Cell viability was measured using WST-1 at 1:10 dilution with CSS-FBS media at absorbance of 450 nm (Tecan 1100 Plate Reader). IC50 dosage was calculated using GraphPad Prism. Each data point was conducted in technical and biological triplicate.

4.3 Synergy studies

Cells were seeded at the densities grown as stated above. Drug combinations used included enzalutamide plus saracatinib and docetaxel plus saracatinib at their respective IC50 dosages for each cell line. Therapy was given, beginning at 2x the IC50 dose, then serial diluted by 2 till 9 dilution groups were established. Cell viability was measured using WST-1 at 1:10 dilution with CSS-FBS media at absorbance of 450 nm (Tecan 1100 Plate Reader). Measured absorbance was converted in percentile and inputted in the Bliss Independence equation (24) as well as CompuSyn 1.1, a computer software that determines synergy *via* Combination Index (25) between drugs based on individual dose response. Bliss independence is calculated as Fab=Fa x Fb, where Fa/b is the fraction of cells affected by drug A/B and Fab is the product of the two fractions, representing the predicted additivity of the two drugs. Bliss independence value is portrayed with Fab and the experimental values of each combination. Combinations with values greater than Fab are considered synergistic, while combination with values less than Fab are considered antagonistic. Each data point was conducted in technical triplicate.

4.4 Immunofluorescence imaging and quantitative image-based cytometry

For cell-cycle analysis of 22Rv1 cells, a quantitative image-based cytometry method was used as described previously (41). Briefly, cells were labeled with 10 μM EdU for 30 min and processed with the Click-IT EdU Alexa Fluor 488 Imaging Kit (Invitrogen, #C10337) according to the manufacturer's instructions. Otherwise cells were extracted with 1x PBS containing 0.1% Triton-X100 for 10 min on ice prior to fixation with 3% paraformaldehyde/2% sucrose for 15 min at ambient temperature. Subsequently, cells were permeabilized with 100% methanol at -20°C for 10 min, blocked in blocking buffer (1x TBS containing 5% BSA, 0.05% Tween-20) for 1 hour, and incubated in primary antibodies for PCNA (mouse, 1:200, Calbiochem #PC10) and γH2AX (rabbit, 1:1000, CST #9718S) in blocking buffer overnight at 4° C. Next day, cells were washed 3 times with PBS-T before incubation with Cy5 anti-rabbit and Cy3 anti-mouse secondary antibodies for 1 hour at ambient temperature. Cells were stained with DAPI before mounting coverslips on slides.

Z-stack images were captured using a Leica DMi8 microscope (Leica Microsystems). Image segmentation of nuclei and whole cells was performed using the cellpose algorithm implemented in Python. The cyto2 and nuclei models were further trained on the images in this study to achieve high-quality segmentation. Nuclear and/or cellular masks were exported to ImageJ to measure total intensity, mean intensity, and pixel areas of defined regions within max-projected images.

4.5 Caspase 3/7 activation

To measure caspase 3/7 activation, Invitrogen CellEvent Caspase-3/7 green detection reagent (C10423, ThermoFisher) was used as stated in manufacturer's protocol. 22Rv1 cells were seeded in 96 well plates at 4,000 cells/ 0.1 ml in FBS media overnight. Media in the wells was then replaced with CSS-FBS media and grown for 3 days. The following drug groups were then administered for 24 hours at IC50 dosage: DMSO Vehicle, enzalutamide, saracatinib, docetaxel, enzalutamide plus saracatinib, docetaxel plus saracatinib. After 24 hours, the caspase reagent, diluted to 4 μM was added to the cells for 1 hour. Fluorescence was observed using Spark Cyto Multimode Plate Reader. Excitation and emission settings were 488 and 590/50 nm respectively. The intensity of fluorescence was analyzed with Spark Cyto Imaging software. Each data point was conducted in biological triplicate.

4.6 Immunoblot analysis

Cells were lysed with RIPA buffer supplemented with protease inhibitor tablets and phosphatase inhibitor cocktail. Protein concentration was quantified using Pierce BCA protein assay kit following manufacturer's protocol. 40 micrograms of protein were loaded into GenScript SurePage 4%-12% polyacrylamide gel, transferred to both nitrocellulose and PVDF membranes, blocked in 5% BSA or 5% milk in 1x TBST for one hour, before incubating the membranes with primary antibodies overnight at 4°C in 1% BSA solution. Membranes were washed with 1x TBST 3 three times before incubating the membranes in LI-COR IR-conjugated secondary antibodies (1:10,000-20,000) for 2 hours at room temperature. Membranes were washed three times with 1x TBST and imaged using the LI-COR Odyssey System. Membranes were adjusted and quantified with the LI-COR Image Studio Lite software (v5.2). The following antibodies were used for Western Blot Analysis: At 1:1000 Total AR (rabbit CST: #5153), Total SRC (rabbit CST: #2109), Total β-actin (mouse Santa Cruz: 4970S), ARpY534 (rabbit Invitrogen: #PA5-64643), SRCpY416 (rabbit CST: #2101), FKBP5 (rabbit CST: #8245), NKX3.1 (rabbit CST: #83700) cleaved PARP (mouse CST: #32563), total PARP (rabbit CST: #9532). At 1:500, ARpS81 (rabbit Sigma-Aldrich: #07-1375), AR-V7 (rabbit CST: #19672). Blots are results in triplicate.

4.7 RNA sequencing and analysis

Total RNA was isolated from 22Rv1 cells *via* RNeasy Mini Kit (QIAGEN, no. 74106). Messenger RNA was purified from total RNA using poly-T oligo-attached magnetic beads. After fragmentation, the first strand cDNA was synthesized using hexamer primers followed by

second strand cDNA synthesis. Library sequencing was conducted on Novaseq6000 S4 flowcell for PE150 sequencing (Novogene Corporation Inc., Sacramento, CA 95817). Transcriptome sequence data processing and analysis were performed using pipelines at the Minnesota Supercomputing Institute (MSI) and University of Minnesota Informatics Institute (UMII) at the University of Minnesota. Raw reads were trimmed, aligned to the GRCh38 human genome, and gene-level read counts were generated using the CHURP pipeline (42). All downstream gene expression analyses and visualizations were conducted using R (4.2.1), RStudio (2022.07.2 + 576) (43) and GraphPad Prism 9. Genes with less than ten total counts across all samples were filtered out. Count normalization was conducted using DESeq2's median of ratios method (44). Visualizations were generated using the R packages ggplot2 (45) and ClassDiscovery (46), and Graphpad Prism 9.

4.8 Gene activity scoring

Relative AR activity scores were computed by summing the normalized counts of the set of genes defining each signature. Peter Nelson's AR signature includes 83 genes, all of which were present in the dataset (29). Scott Dehm's signature includes 19 genes, 18 of which were present in the dataset (30).

4.9 Statistics and analysis

The data were presented as the mean ± SD for the indicated number of independently performed experiments, except the immunofluorescence data, which was presented as the median. The statistical significance ($p<0.05$) was determined using GraphPad Prism 9 with the tests indicated in the figure legends. $P < 0.05$ was considered to indicate a statistically significant difference. P values were determined with significance indicated as follows: *, $P < 0.05$; **, $P < 0.01$; ***, $P < 0.001$; and ****, $P < 0.0001$. Tukey's multiple comparisons test and Kruskal-Wallis test were performed after one-way ANOVA.

Data availability statement

The data presented in the study are deposited in the Gene Expression Omnibus (GEO) repository, accession number GSE229805.

Author contributions

RW and JD conceived the project. RW and VT designed, conducted experiments and analysed data under supervision of JD. MB performed microscopy, quantitative image-based cytometry analysis, and analysed data under the supervision of RW and HD. HB, AD and JH performed RNA sequencing analysis and provided project discussion. RW wrote the manuscript draft with support from JD. All authors provided constructive critiques in editing the manuscript. All authors contributed to the article and approved the submitted version.

Funding

RW is supported by 1F31CA261056-01 through NIH National Cancer Institute. HD is supported by the American Society of Hematology Scholar Award, the National Institutes of Health's National Center for Advancing Translational Sciences, grants KL2TR002492 and UL1TR002494, a grant from the National Heart, Lung, and Blood Institute under award number R01HL163011, and the 2022 AACR Career Development Award to Further Diversity, Equity, and Inclusion in Cancer Research, which is supported by Merck, Grant Number 22-20-68-NGUY. JD is supported by the National Cancer Institute of the National Institutes of Health under award number R01CA269801 and the Department of Defense Prostate Cancer Research Program W81XWH-18-1-0542. The content is solely the responsibility of the authors and does not necessarily represent the official views of the National Institutes of Health.

Acknowledgments

We thank members of the Drake lab for providing advice and input on the manuscript. We also thank Dr. Scott Dehm at the University of Minnesota for his gifts of AD1 and R1D567 cells.

Conflict of interest

JD has no conflicts relevant to this work. However, he holds equity in and serves as Chief Scientific Officer of Astrin Biosciences. This interest has been reviewed and managed by the University of Minnesota in accordance with its Conflict of Interest policies. None of these companies contributed to or directed any of the research reported in this article.

The remaining authors declare that the research was conducted in the absence of any commercial or financial relationships that could be constructed as a potential conflict of interest.

Publisher's note

Supplementary material

The Supplementary Material for this article can be found online at: https://www.frontiersin.org/articles/10.3389/fonc.2023.1210487/full#supplementary-material

References

1. Vance MA, Smith JAJr. Endocrine and clinical effects of leuprolide in prostatic cancer. *Clin Pharmacol Ther* (1984) 36(3):350–4. doi: 10.1038/clpt.1984.186

2. Tran C, Ouk S, Clegg NJ, Chen Y, Watson PA, Arora V, et al. Development of a second-generation antiandrogen for treatment of advanced prostate cancer. *Science* (2009) 324(5928):787–90. doi: 10.1126/science.1168175

3. Scher HI, Fizazi K, Saad F, Taplin ME, Sternberg CN, Miller K, et al. Increased survival with enzalutamide in prostate cancer after chemotherapy. *N Engl J Med* (2012) 367(13):1187–97. doi: 10.1056/NEJMoa1207506

4. Forde PM, Antonarakis ES. Abiraterone for the treatment of advanced prostate cancer. *Int J Target Ther Cancer* (2012) 1(3):40–2.

5. Cairns P, Okami K, Halachmi S, Halachmi N, Esteller M, Herman JG, et al. Frequent inactivation of PTEN/MMAC1 in primary prostate cancer. *Cancer Res* (1997) 57(22):4997–5000.

6. Nelson PS. Molecular states underlying androgen receptor activation: a framework for therapeutics targeting androgen signaling in prostate cancer. *J Clin Oncol* (2012) 30(6):644–6. doi: 10.1200/JCO.2011.39.1300

7. Hossain D, Bostwick DG. Significance of the TMPRSS2:ERG gene fusion in prostate cancer. *BJU Int* (2013) 111(5):834–5. doi: 10.1111/bju.12120

8. Dehm SM, Schmidt LJ, Heemers HV, Vessella RL, Tindall DJ. Splicing of a novel androgen receptor exon generates a constitutively active androgen receptor that mediates prostate cancer therapy resistance. *Cancer Res* (2008) 68(13):5469–77. doi: 10.1158/0008-5472.CAN-08-0594

9. Antonarakis ES, Armstrong AJ, Dehm SM, Luo J. Androgen receptor variant-driven prostate cancer: clinical implications and therapeutic targeting. *Prostate Cancer Prostatic Dis* (2016) 19(3):231–41. doi: 10.1038/pcan.2016.17

10. Scher HI, Lu D, Schreiber NA, Louw J, Graf RP, Vargas HA, et al. Association of AR-V7 on circulating tumor cells as a treatment-specific biomarker with outcomes and survival in castration-resistant prostate cancer. *JAMA Oncol* (2016) 2(11):1441–9. doi: 10.1001/jamaoncol.2016.1828

11. Drake JM, Graham NA, Stoyanova T, Sedghi A, Goldstein AS, Cai H, et al. Oncogene-specific activation of tyrosine kinase networks during prostate cancer progression. *Proc Natl Acad Sci USA* (2012) 109(5):1643–8. doi: 10.1073/pnas.1120985109

12. Drake JM, Paull EO, Graham NA, Lee JK, Smith BA, Titz B, et al. Phosphoproteome integration reveals patient-specific networks in prostate cancer. *Cell* (2016) 166(4):1041–54. doi: 10.1016/j.cell.2016.07.007

13. Cai H, Babic I, Wei X, Huang J, Witte ON. Invasive prostate carcinoma driven by c-src and androgen receptor synergy. *Cancer Res* (2011) 71(3):862–72. doi: 10.1158/0008-5472.CAN-10-1605

14. Varkaris A, Katsiampoura AD, Araujo JC, Gallick GE, Corn PG. Src signaling pathways in prostate cancer. *Cancer Metastasis Rev* (2014) 33(2-3):595–606. doi: 10.1007/s10555-013-9481-1

15. Guo Z, Dai B, Jiang T, Xu K, Xie Y, Kim O, et al. Regulation of androgen receptor activity by tyrosine phosphorylation. *Cancer Cell* (2006) 10(4):309–19. doi: 10.1016/j.ccr.2006.08.021

16. Migliaccio A, Varricchio L, De Falco A, Castoria G, Arra C, Yamaguchi H, et al. Inhibition of the SH3 domain-mediated binding of src to the androgen receptor and its effect on tumor growth. *Oncogene* (2007) 26(46):6619–29. doi: 10.1038/sj.onc.1210487

17. DaSilva J, Gioeli D, Weber MJ, Parsons SJ. The neuroendocrine-derived peptide parathyroid hormone-related protein promotes prostate cancer cell growth by stabilizing the androgen receptor. *Cancer Res* (2009) 69(18):7402–11. doi: 10.1158/0008-5472.CAN-08-4687

18. Dai B, Chen H, Guo S, Yang X, Linn DE, Sun F, et al. Compensatory upregulation of tyrosine kinase Etk/BMX in response to androgen deprivation promotes castration-resistant growth of prostate cancer cells. *Cancer Res* (2010) 70 (13):5587–96. doi: 10.1158/0008-5472.CAN-09-4610

19. Jiang T, Qiu Y. Interaction between src and a c-terminal proline-rich motif of akt is required for akt activation. *J Biol Chem* (2003) 278(18):15789–93. doi: 10.1074/jbc.M212525200

20. Gioeli D, Black BE, Gordon V, Spencer A, Kesler CT, Eblen ST, et al. Stress kinase signaling regulates androgen receptor phosphorylation, transcription, and localization. *Mol Endocrinol* (2006) 20(3):503–15. doi: 10.1210/me.2005-0351

21. Koryakina Y, Ta HQ, Gioeli D. Androgen receptor phosphorylation: biological context and functional consequences. *Endocr Relat Cancer* (2014) 21(4):T131–45. doi: 10.1530/ERC-13-0472

22. Twardowski PW, Beumer JH, Chen CS, Kraft AS, Chatta GS, Mitsuhashi M, et al. A phase II trial of dasatinib in patients with metastatic castration-resistant prostate cancer treated previously with chemotherapy. *Anticancer Drugs* (2013) 24 (7):743–53. doi: 10.1097/CAD.0b013e328361feb0

23. Araujo JC, Trudel GC, Saad F, Armstrong AJ, Yu EY, Bellmunt J, et al. Docetaxel and dasatinib or placebo in men with metastatic castration-resistant prostate cancer (READY): a randomised, double-blind phase 3 trial. *Lancet Oncol* (2013) 14(13):1307–16. doi: 10.1016/S1470-2045(13)70479-0

24. Bliss CI. The calculation of microbial assays. *Bacteriol Rev* (1956) 20(4):243–58. doi: 10.1128/br.20.4.243-258.1956

25. Chou TC. Drug combination studies and their synergy quantification using the chou-talalay method. *Cancer Res* (2010) 70(2):440–6. doi: 10.1158/0008-5472.CAN-09-1947

26. Gordon V, Bhadel S, Wunderlich W, Zhang J, Ficarro SB, Mollah SA, et al. CDK9 regulates AR promoter selectivity and cell growth through serine 81 phosphorylation. *Mol Endocrinol* (2010) 24(12):2267–80. doi: 10.1210/me.2010-0238

27. Chen S, Gulla S, Cai C, Balk SP. Androgen receptor serine 81 phosphorylation mediates chromatin binding and transcriptional activation. *J Biol Chem* (2012) 287 (11):8571–83. doi: 10.1074/jbc.M111.325290

28. Russo JW, Liu X, Ye H, Calagua C, Chen S, Voznesensky O, et al. Phosphorylation of androgen receptor serine 81 is associated with its reactivation in castration-resistant prostate cancer. *Cancer Lett* (2018) 438:97–104. doi: 10.1016/j.canlet.2018.09.014

29. Arora VK, Schenkein E, Murali R, Subudhi SK, Wongvipat J, Balbas MD, et al. Glucocorticoid receptor confers resistance to antiandrogens by bypassing androgen receptor blockade. *Cell* (2013) 155(6):1309–22. doi: 10.1016/j.cell.2013.11.012

30. Shiota M, Fujimoto N, Higashijima K, Imada K, Kashiwagi E, Takeuchi A, et al. Mineralocorticoid receptor signaling affects therapeutic effect of enzalutamide. *Prostate* (2018) 78:1045–52. doi: 10.1002/pros.23661

31. Che M, Chaturvedi A, Munro SA, Pitzen SP, Ling A, Zhang W, et al. Opposing transcriptional programs of KLF5 and AR emerge during therapy for advanced prostate cancer. *Nat Commun* (2021) 12(1):6377. doi: 10.1038/s41467-021-26612-1

32. Nelson PS, Clegg N, Arnold H, Ferguson C, Bonham M, White J, et al. The program of androgen-responsive genes in neoplastic prostate epithelium. *Proc Natl Acad Sci USA* (2002) 99(18):11890–5. doi: 10.1073/pnas.182376299

33. Sharp A, Coleman I, Yuan W, Sprenger C, Dolling D, Rodrigues DN, et al. Androgen receptor splice variant-7 expression emerges with castration resistance in prostate cancer. *J Clin Invest* (2019) 129(1):192–208.

34. Kim SH, Richardson M, Chinnakannu K, Bai VU, Menon M, Barrack ER, et al. Androgen receptor interacts with telomeric proteins in prostate cancer cells. *J Biol Chem* (2010) 285(14):10472–6. doi: 10.1074/jbc.M109.098798

35. Reddy V, Wu M, Ciavattone N, McKenty N, Menon M, Barrack ER, et al. ATM Inhibition potentiates death of androgen receptor-inactivated prostate cancer cells with telomere dysfunction. *J Biol Chem* (2015) 290(42):25522–33. doi: 10.1074/jbc.M115.671404

36. Reddy V, Iskander A, Hwang C, Divine G, Menon M, Barrack ER, et al. Castration-resistant prostate cancer: androgen receptor inactivation induces telomere DNA damage, and damage response inhibition leads to cell death. *PloS One* (2019) 14 (5):e0211090. doi: 10.1371/journal.pone.0211090

37. Mahajan NP, Liu Y, Majumder S, Warren MR, Parker CE, Mohler JL, et al. Activated Cdc42-associated kinase Ack1 promotes prostate cancer progression *via* androgen receptor tyrosine phosphorylation. *Proc Natl Acad Sci USA* (2007) 104 (20):8438–43. doi: 10.1073/pnas.0700420104

38. Lee LF, Louie MC, Desai SJ, Yang J, Chen HW, Evans CP, et al. Interleukin-8 confers androgen-independent growth and migration of LNCaP: differential effects of tyrosine kinases src and FAK. *Oncogene* (2004) 23(12):2197–205. doi: 10.1038/sj.onc.1207344

39. Plana D, Palmer AC, Sorger PK. Independent drug action in combination therapy: implications for precision oncology. *Cancer Discov* (2022) 12(3):606–24. doi: 10.1158/2159-8290.CD-21-0212

40. Nyquist MD, Li Y, Hwang TH, Manlove LS, Vessella RL, Silverstein KA, et al. TALEN-engineered AR gene rearrangements reveal endocrine uncoupling of androgen receptor in prostate cancer. *Proc Natl Acad Sci USA* (2013) 110(43):17492–7. doi: 10.1073/pnas.1308587110

41. Toledo LI, Altmeyer M, Rask MB, Lukas C, Larsen DH, Povlsen LK, et al. ATR prohibits replication catastrophe by preventing global exhaustion of RPA. *Cell* (2013) 155(5):1088–103. doi: 10.1016/j.cell.2013.10.043

42. Baller J, Kono T, Herman A, Zhang Y. (2019). CHURP: a lightweight CLI framework to enable novice users to analyze sequencing datasets in parallel, in: *Proceedings of the Practice and Experience in Advanced Research Computing on Rise of the Machines (learning)*, 96:1-5. Chicago, IL, USA: Association for Computing Machinery. doi: https://doi.org/10.1145/3332186.3333156

43. Team R. *RStudio: integrated development environment for r*. Boston, MA: Posit PBC (2022).

44. Love MI, Huber W, Anders S. Moderated estimation of fold change and dispersion for RNA-seq data with DESeq2. *Genome Biol* (2014) 15(12):550. doi: 10.1186/s13059-014-0550-8

45. Wickham H. *ggplot2: elegant graphics for data analysis*. NY: Springer New York (2016). Available at: https://cran.r-project.org/web/packages/ClassDiscovery/.

46. Coombes K. *ClassDiscovery: classes and methods for "Class discovery" with microarrays or proteomics r package version 3.4.0*. (2021).